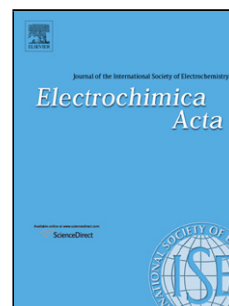


## Accepted Manuscript

Title: Electrochemical characterization of reduced graphene oxide-coated polyester fabrics.

Authors: J. Molina, J. Fernández, J.C. Inés, A.I. del Río, J. Bonastre, F. Cases



PII: S0013-4686(13)00103-5  
DOI: doi:10.1016/j.electacta.2013.01.071  
Reference: EA 19878

To appear in: *Electrochimica Acta*

Received date: 17-10-2012  
Revised date: 8-1-2013  
Accepted date: 15-1-2013

Please cite this article as: J. Molina, J. Fernández, J.C. Inés, A.I. del Río, J. Bonastre, F. Cases, Electrochemical characterization of reduced graphene oxide-coated polyester fabrics., *Electrochimica Acta* (2010), doi:10.1016/j.electacta.2013.01.071

This is a PDF file of an unedited manuscript that has been accepted for publication. As a service to our customers we are providing this early version of the manuscript. The manuscript will undergo copyediting, typesetting, and review of the resulting proof before it is published in its final form. Please note that during the production process errors may be discovered which could affect the content, and all legal disclaimers that apply to the journal pertain.

**Electrochemical characterization of reduced graphene oxide-coated polyester fabrics.**

J. Molina, J. Fernández, J.C. Inés, A.I. del Río, J. Bonastre, F. Cases<sup>1\*</sup>

*Departamento de Ingeniería Textil y Papelera, EPS de Alcoy, Universitat Politècnica de València, Plaza Ferrándiz y Carbonell s/n, 03801 Alcoy, Spain*

**Abstract**

Reduced graphene oxide (RGO) coated fabrics were obtained by chemical reduction of GO on polyester (PES) fabrics. Conducting fabrics that have different applications were obtained by applying several layers of RGO. Electrochemical techniques not traditionally used for the characterization of these materials were used to test their electrical and electrochemical properties. Electrochemical impedance spectroscopy was used to measure the electrical properties. The resistance of the original PES was more than  $10^{11} \Omega \cdot \text{cm}^2$ , but when coated with three RGO layers, the resistance decreased to  $23.15 \Omega \cdot \text{cm}^2$ . Phase angles changed from  $90^\circ$  for PES and PES-GO (capacitive behavior) to  $0^\circ$  for all the RGO coated samples (resistive behavior). Electro-activity was measured by cyclic voltammetry (CV) and scanning electrochemical microscopy. An increase in electro-activity was observed when the inactive GO was reduced to RGO. With CV an increase of electro-activity was observed with an increasing number of RGO layers. The contact between the different RGO sheets is responsible for the electric conduction in the fabrics. The techniques used showed that with only one RGO

---

<sup>1</sup> ISE member

coating, the contact between the RGO sheets is not good and more coatings were needed to assure good electrical and electrochemical properties.

**Keywords:** Graphene, graphene oxide, conducting fabric, polyester, scanning electrochemical microscopy.

---

\* Corresponding author. Fax.: +34 966528438; telephone: +34 966528412. E-mail address: [fjcases@txp.upv.es](mailto:fjcases@txp.upv.es) (Prof. F. Cases).

## 1. Introduction

Graphene has attracted a great deal of attention during recent years due to its electronic, mechanical and thermal properties, as well as other exciting properties [1-8]. Different methods have been used for the production of graphene [7-9], and mechanical exfoliation was the first method used to produce graphene layers [1]. However, the production by this method is not very effective, so other methods such as chemical vapor deposition or chemical methods have been developed [7-9]. The use of graphene composites with other materials has been also proposed as an alternative solution to the large-scale production of graphene-based materials [10].

In this paper we have used a chemical method to obtain graphene-coated fabrics, where graphene oxide (GO) is reduced chemically to obtain reduced graphene oxide (RGO) on the surface of the fabrics. Textile materials have several advantages over conventional materials such as film, such as having good flexibility and mechanical properties. In addition, they are light materials that have a large surface area. This large surface area makes these materials good substrates on which to deposit other materials for different

applications. For example fabrics have been coated with conducting polymers to produce conductive fabrics [11, 12], with silver or  $\text{TiO}_2$  nanoparticles to produce antibacterial fabrics [13], with single walled nanotubes and  $\text{MnO}_2$  [14] or graphene and  $\text{MnO}_2$  [15] to produce super-capacitors, etc.

Graphene-coated fabrics have usually been obtained by placing the fabrics in contact with solutions containing GO [16, 17]. GO sheets are adsorbed on the surface of the fabrics due to the attraction forces between the functional groups of the fabrics and the oxidized groups of the GO sheets. The process is similar to a dyeing process where an adsorption process occurs [16]. Once the fabric is coated with GO, it is then reduced to RGO using reducing agents such as sodium hydrosulfite [16], hydrazine [17], etc. GO coated fabrics have also generated interest due to the photo-catalytic activity of GO and also to its antibacterial activity [18]. Directly coated graphene fabrics have also been obtained in other works referenced in the bibliography [15]. Graphene fabrics have also been produced by depositing graphene by chemical vapor deposition on a Cu mesh, after which the Cu mesh was dissolved by an acid solution and graphene fabrics were obtained [19]. Regarding graphene fibers, different methods such as wet spinning [20] or obtaining hydrothermally [21] using GO as a precursor material have been used in the past. The fibers formed were later reduced chemically [20] or thermally [21] to obtain graphene fibers.

The fibers used to deposit graphene or GO have been polyarylate [16] or cotton [17]. Polyester (PES) is one of the most used fibers in industry so it would be of interest to use it to study the production of graphene-coated fabrics. In addition, the presence of polar groups on its structure makes this family attractive because the adhesion of GO is better in fibers with polar groups (C-O and C=O groups are present in PES).

In the present work, graphene-coated fabrics were obtained by reducing GO on the surface of the fabrics. Traditional characterization techniques such as Fourier transform infrared spectroscopy with total attenuated reflection (FTIR-ATR) were used for chemical characterization, while scanning electron microscopy (SEM) was used to observe the morphology of the coatings and the samples. There is a lack of characterization of these materials by electrochemical techniques, so electrochemical techniques not usually used for the characterization of these materials were used in this work. Electrochemical impedance spectroscopy (EIS) was used for the measurement of the electrical resistance ( $\Omega \cdot \text{cm}^2$ ) and the surface resistivity ( $\Omega/\square$ ) of the fabrics and also to obtain the phase angle ( $^\circ$ ), which gives an indication of the insulating/conducting behavior of the fabrics. Scanning electrochemical microscopy (SECM) was used to measure the electrochemical activity by means of approach curves. SECM is a relatively novel (1989) and powerful technique that is becoming more popular among researchers [22-24]. Its applications range for example from the study of corrosion of metals [25] to the study of biological systems [23]. Cyclic voltammetry (CV) was also used to measure the electro-activity of these materials.

## 2. Experimental

### 2.1. Reagents and materials

All reagents used were of analytical grade. Sodium dithionite ( $\text{Na}_2\text{S}_2\text{O}_4$ ) and sulphuric acid ( $\text{H}_2\text{SO}_4$ ) were supplied by Merck. Hexaammineruthenium (III) chloride ( $\text{Ru}(\text{NH}_3)_6\text{Cl}_3$ ) 98% and potassium chloride (KCl), were used as received from Acrös Organics and Merck respectively.

Monolayer GO powders were supplied by Nanoinnova Technologies S.L. (Spain).

PES fabrics were supplied by Viatex S.A. and their characteristics were: fabric surface density,  $140 \text{ g}\cdot\text{m}^{-2}$ ; warp threads per cm, 20 (warp linear density, 167 dtex); weft threads per cm, 60 (weft linear density, 500 dtex). These are specific terms used in the field of textile industry and their meaning can be consulted in a textile glossary [26]. The estimated diameter of polyester fibers was around  $17 \mu\text{m}$  (estimated employing SEM). The effective area of the fabric was also estimated employing the values of density ( $1.37 \text{ g}\cdot\text{cm}^{-3}$ ), fabric surface density and diameter of the fibers. The value obtained was around  $24 \text{ cm}^2$  per geometrical  $\text{cm}^2$  of the fabric.

Where necessary, solutions were deoxygenated by bubbling nitrogen ( $\text{N}_2$  premier X50S). Ultrapure water was obtained from an Elix 3 Millipore-Milli-Q Advantage A10 system with a resistivity near to  $18.2 \text{ M}\Omega \text{ cm}$ .

## 2.2. Synthesis of RGO on PES fabrics

RGO coated fabrics were obtained with the same method used by Fugetsu et al. [16]. Solutions of  $3 \text{ g}\cdot\text{L}^{-1}$  of GO were prepared by mixing monolayer GO powders with water in an ultrasound bath for 30 minutes. Then the PES fabric was placed in contact with the GO solution for 30 minutes to allow the dyeing of the fabric. Fabrics were allowed to dry for 24 h. After this time, they were placed for 30 min in a solution containing sodium dithionite at approximately  $90^\circ \text{C}$  to perform the reduction of GO to RGO. Finally, the fabrics were washed several times with ultrapure water. RGO powders from solution were also filtered to perform FTIR-ATR measurements in order to assure the reduction of GO to RGO. Several samples with a different number of RGO coatings (1, 2, 3, 4) were obtained (PES-G1, PES-G2, PES-G3, PES-G4) repeating the same procedure mentioned above. One sample coated with GO (PES-GO) was also obtained for comparison of the different results.

### 2.3. FTIR-ATR

FTIR-ATR with horizontal mono-rebound attenuated total reflection was performed with a Nicolet 6700 Spectrometer equipped with deuterated triglycine sulfate detector. An accessory with pressure control was used to equalize the pressure in the different solid samples. A prism of ZnSe was used. Spectra were collected with a resolution of  $4\text{ cm}^{-1}$  and 100 scans were averaged for each sample. GO and RGO powders were characterized. PES fabrics uncoated and coated with GO and RGO were also characterized by FTIR-ATR.

### 2.4. SEM

A Jeol JSM-6300 scanning electron microscope was used to observe the morphology of the samples. SEM analyses were performed using an acceleration voltage of 10 kV. Samples for SEM measurements were coated with Au using a sputter coater Bal-Tec SCD 005.

### 2.5. Electrical measurements

An Autolab PGSTAT302 potentiostat/galvanostat was used to perform EIS analyses. EIS measurements were performed in the  $10^5$ - $10^{-2}$  Hz frequency range. The amplitude of the sinusoidal voltage used was  $\pm 10\text{ mV}$ . Measurements were carried out in a two-electrode arrangement. Two types of configuration were used to carry out the measurements. In the first one, the sample was located between two round copper electrodes ( $A = 1.33\text{ cm}^2$ ), while in the second configuration, two rectangular copper electrodes ( $0.5\text{ cm} \times 1.5\text{ cm}$ ) separated by  $1.5\text{ cm}$  and pressed on the fabric sample were used. The measured area of the fabric with this configuration was a square of  $1.5\text{ cm}$  so

the measured impedance modulus ( $\Omega$ ) was equal to the surface resistivity ( $\Omega/\square$ ) [27, 28].

## 2.6. CV

An Autolab PGSTAT302 potentiostat/galvanostat was used to perform CV measurements of the RGO coated fabrics in 0.5 M  $\text{H}_2\text{SO}_4$  solutions. The conducting fabric sample was located between two Ti plates to connect the sample with the potentiostat/galvanostat. The measurements were performed in a three-electrode arrangement. The counter electrode used was made of stainless steel; the pre-treatment consisted of polishing, degreasing with acetone in an ultrasonic bath and washing with water in the ultrasonic bath. The working electrode was made by cutting a strip of the RGO coated conducting fabric, the exposed area of the fabric to the solution was  $1 \text{ cm}^2$ . Potential measurements were referred to Ag/AgCl (3 M KCl) reference electrode. Oxygen was removed from solution by bubbling nitrogen gas for 10 min and then a  $\text{N}_2$  atmosphere was maintained during the measurements. The ohmic potential drop was measured and introduced in the Autolab software (GPES). The measurements were done between -0.2 V and +0.8 V. The characterization by means of CV has been taken at different scan rates as previous authors have corroborated the influence of this parameter on the electrochemical response obtained [11, 27]. The scan rates used were  $50 \text{ mV}\cdot\text{s}^{-1}$ ,  $5 \text{ mV}\cdot\text{s}^{-1}$  and  $1 \text{ mV}\cdot\text{s}^{-1}$ .

## 2.7. SECM

SECM measurements were carried out with a Sensolytics scanning electrochemical microscope. The three-electrode cell configuration consisted of a  $100\text{-}\mu\text{m}$ -diameter Pt SECM-tip, a Pt wire auxiliary electrode and an Ag/AgCl (3 M KCl) reference electrode.

The solution selected for the measurements was an aqueous solution of 0.01 M  $\text{Ru}(\text{NH}_3)_6\text{Cl}_3$  (redox mediator) with 0.1 M KCl. All the experiments were carried out in an inert nitrogen atmosphere. The substrates were the different fabrics obtained, and these substrates were then glued to microscope slides with epoxy resin. The dimensions of the samples employed were  $0.5 \text{ cm} \times 0.5 \text{ cm}$  ( $0.25 \text{ cm}^2$ ). The SECM-tip was moved in z direction and the tip current was recorded to obtain the approach curves. Approach curves give us an indication of the electro-activity of the surface. These curves were compared to the theoretical ones (positive and negative feedback models). Experimental approach curves were shifted to adjust with the theoretical ones to calculate the real distance between the sample and the SECM-tip. After that the electrode was positioned at the desired height to carry out the constant-height SECM images in the plane xy. The substrate surfaces in all the measurements were at their open circuit potential (OCP).

### 3. Results and discussion

#### 3.1. FTIR-ATR

FTIR-ATR measurements were performed to characterize GO powders as well as the RGO powders obtained after chemically reducing GO. Fig. 1 shows the spectra of GO and RGO. GO powders present different bands arising from oxidized groups. The band around  $1720 \text{ cm}^{-1}$  was attributed to stretching vibrations from C=O [29-31]. The peak at  $1613 \text{ cm}^{-1}$  was attributed to C=C from unoxidized  $\text{sp}^2$  bonds [29-31]. The band at  $1220 \text{ cm}^{-1}$  was assigned to C-OH stretching vibrations [29], and the band around  $1050 \text{ cm}^{-1}$  arises from C-O stretching vibrations [29, 31]. When GO was reduced to RGO, all the peaks arising from oxidized groups were substantially reduced, indicating a reduction of

the oxygen content in the sample, although they were not completely removed. The reduction of oxygen below a certain level is not really feasible because it is difficult to remove remaining hydroxyl groups [32]. RGO powders showed a band at  $1562\text{ cm}^{-1}$ , this band has been attributed to skeletal vibration of graphene sheets [33]. When GO and RGO were deposited on PES fabrics, no substantial variation was observed in the original spectra of PES; only a slight decrease of the different bands of PES was observed (Figures not shown). The majority of bands of GO and RGO coincide with that of PES and the different contributions cannot be properly discerned.

### 3.2. SEM

SEM was used to observe the morphology of the coatings obtained. Fig. 2 shows the different micrographs obtained for the different RGO coated fabrics. Fig. 2-a,b show micrographs of the PES-1G sample. In these two micrographs RGO sheets deposited on PES fibers can be seen. In general, it is very difficult to observe these sheets; however the folds created during the deposition process in some of these sheets help to locate them. The dimensions of the RGO sheets are about  $4\text{-}6\text{ }\mu\text{m}$  in length. An increase in the number of coatings (samples PES-2G, PES-3G, PES-4G) produced an increase in the RGO content, however it was more difficult to locate the RGO sheets since they could not be distinguished from the fibers. Fig. 2-c,d show micrographs of the PES-4G sample, where the presence of some particles can be observed on the surface of the fibers. The values of the impedance modulus obtained with the electrical measurements (section 3.3) indicated that the deposition of 4 coatings of RGO produced a decrease of more than 9 orders of magnitude when compared with PES. So the fibers with 4 coatings would be completely coated with RGO, despite our not being able to observe

them. Fig. 2-c shows also the structure of the fabric, with the warp and weft at different heights. The estimated diameter of the fibers by SEM micrographs was around 17  $\mu\text{m}$ .

### 3.3. Electrical measurements

EIS was used to measure the electrical resistance ( $\Omega\cdot\text{cm}^2$ ) of the different samples obtained as well as their phase angle ( $^\circ$ ); the latter measurement gives an indication of the insulating/conducting behavior of the fabrics. Fig. 3 shows the Bode plots for the different fabrics measured. Samples of PES and PES coated with GO were also measured to compare the different values obtained. Conducting fabrics with 1, 2, 3 and 4 RGO deposition processes were measured.

In Fig. 3-a, the impedance modulus ( $|Z|$ ) at the different frequencies for the different samples can be observed. PES fabrics present values of  $|Z|$  higher than  $10^{11}$   $\Omega\cdot\text{cm}^2$  for low frequencies. When the sample was coated with GO,  $|Z|$  was not substantially modified and similar values were obtained. GO is an insulating material due to the disrupted  $\text{sp}^2$  bonding networks [34], however when the sample of PES coated with GO was reduced, a decrease of  $|Z|$  of about seven orders of magnitude was obtained (26014  $\Omega\cdot\text{cm}^2$  for 0.01 Hz). Fig. 4 shows the dependence of  $|Z|$  on ac frequency for the different samples so that the changes can be properly observed. When another layer of RGO was deposited on the fabric (PES-2G),  $|Z|$  lowered to 700  $\Omega\cdot\text{cm}^2$  for 0.01 Hz. The third layer of RGO produced also a decrease of  $|Z|$  to 23.15  $\Omega\cdot\text{cm}^2$  for 0.01 Hz. However the fourth coating did not produce a decrease in  $|Z|$  and around 29.4  $\Omega\cdot\text{cm}^2$  for 0.01 Hz was measured. As mentioned previously, Fig. 4 shows the dependence of  $|Z|$  on ac frequency for the different samples of PES coated with RGO. The values of  $|Z|$  can be observed with the varying frequency. It is worth mentioning that the values of  $|Z|$  increase with the decreasing frequency for the PES-1G sample. This would indicate a poor contact

between the RGO sheets (slight capacitive behavior). On the other hand, the samples with more coatings of RGO (PES-2G, PES-3G, PES-4G) showed a decrease of  $|Z|$  with the decreasing frequency, this would indicate a slight inductive behavior. From the first to the third coating there is an increase of the conductivity of the fabrics due to the improved contact between the RGO sheets. In the first coating, part of the RGO layers may not be in contact so that electrical conduction is more difficult. Another layer of RGO allows the contact between the isolated sheets. CV measurements showed similar results, confirming the better contact with more coatings of RGO (section 3.4). After three deposits the limit of conductivity was reached and more layers did not produce an increase in the conductivity.

Fig. 3-b shows the data for the phase angle at the different frequencies. PES presents a phase angle of about  $90^\circ$ , a typical value of an insulating material that acts as a capacitor (data at low frequencies is not presented since noise due to the large values of impedance modulus was observed). For the sample of PES coated with GO, the same phase angle was obtained indicating no substantial modification of its electrical properties by the GO layer, the PES-GO sample also acted as an electrical insulator. However, for all the samples coated with RGO (PES-1G, PES-2G, PES-3G and PES-4G),  $0^\circ$  phase angles were obtained in the majority of the frequency range, indicating that the fabrics behaved like conducting materials, showing a resistive behavior.

The values of surface resistivity ( $\Omega/\square$ ) were obtained with the second electrode configuration; two rectangular copper electrodes (0.5 cm x 1.5 cm) separated by 1.5 cm and pressed on the fabric sample. The values of surface resistivity obtained were  $1.6 \cdot 10^7 \Omega/\square$  (PES-1G),  $2.94 \cdot 10^5 \Omega/\square$  (PES-2G),  $11.06 \cdot 10^3 \Omega/\square$  (PES-3G) and  $20.85 \cdot 10^3 \Omega/\square$  (PES-4G). The tendency obtained was similar to that observed with the first electrode configuration with a decrease of the surface resistivity until the third coating process.

These values of surface resistivity would make these fabrics appropriate as antistatic materials. Static charging on the surface of the fabrics is excluded with surface resistivity below  $5 \cdot 10^9 \Omega/\square$  [35], so even the sample coated with one layer of RGO would be adequate for this purpose.

### 3.4. CV

Fig. 5 shows the voltammograms obtained for PES-1G and PES-3G samples. Fig. 5-a shows the voltammogram obtained for the PES-1G sample. With only one deposition process the voltammogram obtained showed a linear behavior (indicating a resistive response) with a current density value of about  $-1.4 \text{ nA} \cdot \text{cm}^{-2}$  at  $-0.2 \text{ V}$  for  $50 \text{ mV} \cdot \text{s}^{-1}$ . Different scan rates were also used to test the electro-activity of the fabrics ( $50$ ,  $5$  and  $1 \text{ mV} \cdot \text{s}^{-1}$ ), obtaining the same resistive voltammogram for all the scan rates used. Fig. 5-b shows the voltammograms obtained for the PES-3G sample. The higher scan rate ( $50 \text{ mV} \cdot \text{s}^{-1}$ ) produced a current density of around  $-30 \mu\text{A} \cdot \text{cm}^{-2}$  at  $-0.2 \text{ V}$ . The current density obtained with 3 deposition processes (PES-3G) was more than 4 orders of magnitude higher than that obtained for the sample with only one deposition process (PES-1G). In this case it can be seen that the scan rate has some influence on the electrochemical behavior. With the scan rate of  $1 \text{ mV} \cdot \text{s}^{-1}$ , the form of the voltammogram was more similar to voltammograms obtained for graphene [36]. Also the electrical charge and current densities of the voltammogram increased with the decreasing scan rate. This behavior has not been observed in the bibliography since the normal trend is an increase of the charge and current density with the increasing scan rate [36, 37]. The explanation for this fact could be the nature of the sample. Samples of graphene are normally studied in isolation [36, 37] or are deposited on conducting substrates such as metals where the charge transfer between the metal and graphene is instantaneous. However in

conducting fabrics, RGO is deposited on PES, which is an insulating material. So charge transfer has to be produced on the RGO sheets. The electrical contact from the top to the bottom of the sample is produced through the contact of the different RGO sheets. For example for a 1 cm length sample, if the average size of the RGO sheets were 10  $\mu\text{m}$  (the real size is lower as has been observed in SEM micrographs), at least 1000 RGO sheets would be needed to produce the electrical contact between the top and the bottom of the fabric (the case for a monolayer smooth sample). This number increases in the case of the fabrics which present a 3D structure, where different fibers and yarns compose the fabrics. The charge transfer is slow since it has to proceed through the RGO sheets. If the scan rate is too fast ( $50 \text{ mV}\cdot\text{s}^{-1}$ ), there is no sufficient time to produce the oxidation and reduction of RGO sheets and a resistive response was obtained. When the scan rate decreased to  $5 \text{ mV}\cdot\text{s}^{-1}$ , there was more time to produce the oxidation and reduction of the RGO sheets and this is why there was an increase of the electrical charge and current density in the voltammograms. The lowest scan rate ( $1 \text{ mV}\cdot\text{s}^{-1}$ ) produced a higher increase of the electrical charge and current densities reached since there was even more time to produce the oxidation and reduction of RGO sheets. With only one deposition process (PES-1G), it was not possible to observe the redox processes even with the lowest scan rate ( $1 \text{ mV}\cdot\text{s}^{-1}$ ). This was attributed to the fact that there were not enough RGO sheets in the coating to produce a proper contact between them and only the characteristic resistive response was observed. The results obtained in CV were in agreement with those observed in EIS, where the same trend was observed. Fig. 5-c shows the voltammograms obtained for the PES-3G sample at different scan rates, however in this case the ohmic resistance was measured and compensated. It was observed that this compensation is necessary for materials that have an ohmic resistance such as conducting polymer-coated fabrics [11, 27]. PES-1G sample had such a high

resistance that it was not possible to compensate it, and for this reason it was not compensated in Fig. 5-a. Fig. 5-b was also done without compensation to compare it with Fig. 5-a under the same conditions. Comparing the voltammograms without (Fig. 5-b) and with compensation (Fig. 5-c), an increase in the electrical charge and the current density compared to Fig. 5-b can be seen.

### 3.5. SECM.

Approach curves were obtained by SECM measurements to test the electro-activity of the conducting fabrics. Approach curves give an indication of the electro-activity of the sample surface. The SECM-tip is negatively polarized to reduce the oxidized (Ox) form of the redox mediator at a diffusion controlled rate ( $i_{\infty}$ ). The reduction current obtained ( $i$ ) is measured at the SECM-tip. In our case we used  $\text{Ru}(\text{NH}_3)_6^{3+}$  (Ox) as redox mediator and it was reduced to  $\text{Ru}(\text{NH}_3)_6^{2+}$  (Red) at the SECM-tip at a potential of -0.4 V (vs. Ag/AgCl 3 M KCl). There can be different outcomes, depending on the conductivity of the substrate and the distance between the SECM-tip and the substrate:

- !! When the SECM-tip is sufficiently far from the substrate there is no impediment for the diffusion of oxidized species (Ox) to be reduced on the surface of the SECM-tip, the current measured in this case is the diffusion current ( $i_{\infty}$ ).
- !! If the surface is non conductive, when the SECM-tip approaches the substrate there is a hindrance to the diffusion of oxidized species (Ox) to be reduced on the tip. This is caused by the insulating substrate and causes a decrease of the current measured, in this case the current measured  $i < i_{\infty}$ . This situation is known as negative feedback [22].
- !! On the other hand, if the electrode is conductive, when the electrode approaches the surface, there is an increase in oxidized species (Ox) of the mediator. The

surface of the conducting material is able to oxidize the reduced form (Red) of the mediator. This causes an increase in oxidized species (Ox) and the consequent increase of the reduction current measured at the SECM-tip, in this case  $i > i_{\infty}$ . This case is known as positive feedback [22].

In approach curves, the normalized current registered at the SECM-tip ( $I$ ) is represented vs. the normalized distance ( $L$ ). The normalized current is defined as follows:  $I=i/i_{\infty}$ .  $i$  is the current measured at each normalized distance  $L$ .  $i_{\infty}$  is the diffusion current defined as  $i_{\infty}=4 \cdot n \cdot F \cdot D \cdot a \cdot C$ , in which:  $n$  is the number of electrons involved in the reaction;  $F$  is the Faraday constant;  $D$  is the diffusion coefficient;  $a$  is the radius of the SECM-tip and  $C$  is the concentration of the reactant. The normalized currents depend on  $RG$  ( $RG=R_g/a$ , where  $R_g$  is the radius of the insulating glass surrounding the Pt tip of radius “ $a$ ”) and the normalized distance  $L$ ; where  $L=d/a$  ( $d$  is the SECM-tip -substrate separation). The  $RG$  of the SECM-tip used in this work was  $RG \geq 20$ . According to Rajendran et al. [38], Pade’s approximation gives a close and simple equation with less relative error for all distances and is valid for  $RG > 10$ . The approximate expression of the steady-state normalized current assuming positive feedback for finite conductive substrate together with finite insulating glass thickness is:

$$I^c = \frac{1 + \frac{1.5647}{L} + \frac{1.316855}{L^2} + \frac{0.4919707}{L^3}}{1 + \frac{1.1234}{L} + \frac{0.626395}{L^2}} \quad (1)$$

The selection of the expression for the normalized tip current assuming negative feedback was based on the equation for a  $RG=20$  and  $L$  range 0.4-20 [39]:

$$I^{NS} = \frac{1}{0.3554 + \frac{2.0259}{L} + \frac{0.62832}{L^2} \exp\left(-\frac{2.55622}{L}\right)} \quad (2)$$

Approach curves predicted for pure positive and negative feedback calculated from equations 1 and 2 have been also included in the different figures to compare the empirical data with the theoretical models.

A 100  $\mu\text{m}$  Pt SECM-tip held at a potential of -0.4 V (vs. Ag/AgCl 3 M KCl) was used as the working electrode. According to the voltammograms obtained with the SECM-tip in the working solution (Fig. 6), this potential was selected to reduce the oxidized form of the mediator,  $\text{Ru}(\text{NH}_3)_6^{3+}$ , at a diffusion-controlled rate. The approach (I-L) curves obtained for PES and PES-GO are shown in Fig. 7. As can be seen, as the SECM-tip approaches the surface of the PES sample, there is a decrease in the normalized current ( $I < 1$ ), indicating negative feedback. PES is an insulating material and is not able to reoxidize the reduced form of the mediator. GO approach curves have not been obtained in previous works to the best of our knowledge. When GO was deposited on PES fabrics similar behavior was observed. Three measurements obtained in different parts of the fabrics are shown and in all of them negative feedback was obtained. The deposit of GO did not significantly affect the nature of PES sample. We have to take into account that GO is also an insulating material due to the disrupted  $\text{sp}^2$  structure [34] as we have seen previously in EIS measurements. The negative feedback model is also presented for comparison of the experimental curves with the theoretical one.

Fig. 8 shows different approach curves obtained in different parts of the fabric for PES-1G (a) and PES-4G (b) samples. As can be seen in Fig. 8-a, the behavior changes completely from PES-GO. In this case when the SECM-tip approaches the surface of the sample, there is an increase in the normalized current ( $I > 1$ ). This indicates that the sample is electro-active, since the sample is able to reoxidize the reduced form of the redox mediator. Averaged values of positive feedback around 1.3 were obtained for  $L=0.6$ . In Fig. 8-b analyses on the sample of PES-4G are shown. In this case positive

feedback was also obtained and averaged values of 1.4 were obtained for  $L=0.6$ . The positive feedback model is also presented for comparison with the theoretical model. There is little difference when the sample is coated 1, 2, 3 or 4 times with the same procedure (PES-1G, PES-2G, PES-3G, PES-4G). In this case the experiments were done at OCP (sample is not polarized), so only the degree of coverage of the sample by RGO can have influence on the electrochemical response obtained. The electrical contact between the different RGO sheets does not play a role in this case, however, it had significant effect on the electrical conductivity measured by EIS and the electroactivity measured by CV as was commented previously. There has been little previous work on graphene materials using SECM [40-42]. Similar values of positive feedback were obtained for graphene obtained by vapour deposition using a FeMeOH redox mediator, which has a high heterogeneous electron transfer rate [40]. Future work is currently being carried out to study the electrochemical activity of the samples by SECM in polarization conditions.

The main reason why the 100  $\mu\text{m}$  diameter tip was selected to carry out the measurements was the irregular topography of the fabric. The employment of Pt SECM-tips of 100  $\mu\text{m}$  of diameter allows to be positioned at a distance sufficiently high (and inside the influence of the field) to perform an array scan and at the same time avoid the impact of the SECM-tip with the weft. The measured thickness of the fabric (with a micrometer) was 170  $\mu\text{m}$ , so the difference of height between the warp and weft would be around 57  $\mu\text{m}$  (170  $\mu\text{m}$  / 3). For instance, if we take the positive feedback model, to produce a sufficiently intense current signal in the approach curve ( $I$  around 1.4), values of  $L < 1$  are needed. If we had employed a 10  $\mu\text{m}$  diameter tip, the distance between the tip and the sample would be lower than 10  $\mu\text{m}$ . This small gap could produce the impact between the tip and the fabric. Even small variations of height between the different

parts of the fabric when gluing the sample to the glass slide could cause the tip to touch the sample. In addition, if we had employed lower diameter tips, we would have not been able to detect the signal produced by the warp, due to the big difference of height between warp and weft. Then the 100  $\mu\text{m}$  diameter SECM-tip was the best solution for the study of the fabrics.

One main application of the SECM technique is scanning surfaces to obtain 2D and 3D images of the electrochemical activity of the surface of the samples [22, 40]. To obtain these representations the surface of the sample is scanned at a constant height within the influence of the substrate at an initial height of 40  $\mu\text{m}$  above the sample. Our aim was not characterize individually the fibers of the fabric (the diameter of the SECM-tip was 100  $\mu\text{m}$ , so fibers cannot be resolved properly since its diameter is around 17  $\mu\text{m}$ ). The purpose was to observe if RGO was well distributed on the surface of the fabrics. And finally make a comparison between samples coated with RGO and GO to see the different behavior (positive feedback vs. negative feedback, respectively).

Fig. 9-a and Fig. 9-b show the 3D and 2D representation, respectively, of the electroactivity of the PES-1G sample. As can be seen, all the parts of the fabric present normalized current values  $I > 1$  (positive feedback) indicating that the sample is completely coated with RGO. The difference between darker and lighter zones can be attributed to the morphology that the fabric presents, with zones of different height (warp and weft). In this case, the topography of the fabric has more influence than local differences of electroactivity. Fig. 10 shows a superposition of the 2D SECM array and a SEM micrograph for a PES-1G sample. As can be seen, the darker zones coincide with the weft (zones with higher elevation) and the lighter zones with the warp (zones with lower height). The difference is obvious if we compare the results of PES-1G sample with the sample of PES-GO (Fig. 9-c,d). In the latter case, normalized current

values  $I < 1$  (negative feedback) can be seen on the whole fabric. This indicates the insulating nature of the sample. In the case of PES-GO, the more elevated parts of the fabric (weft) produce the lowest values of negative feedback since they are closer to the SECM-tip and the diffusion of redox species is hindered.

#### 4. Conclusions

Polyester (PES) fabrics were coated with graphene oxide (GO) and later it was reduced through a chemical method to obtain reduced graphene oxide (RGO). Samples with a different number of coatings were obtained and analyzed. Fourier transform infrared spectroscopy showed the diminution of the bands attributed to oxidized groups after reducing GO to RGO. Scanning electron microscopy allowed the observation of sheets of RGO deposited on PES fibers, although in general it was very difficult to observe the coatings formed. Electrochemical impedance spectroscopy (EIS), cyclic voltammetry (CV) and scanning electrochemical microscopy (SECM) showed the effective reduction of GO to RGO. With EIS a decrease of the electrical resistance of about 7 orders of magnitude was observed when the fabric of PES-GO was reduced to PES-1G. EIS measurements have also shown a progressive reduction in electrical resistance and surface resistivity with the number of coatings. With three coatings the minimum electrical resistance ( $23.15 \Omega \cdot \text{cm}^2$ ) and surface resistivity ( $1.1 \cdot 10^4 \Omega/\square$ ) were reached. More coatings did not produce a significant improvement in the electrical properties. The surface resistivity obtained with only one RGO coating ( $1.6 \cdot 10^7 \Omega/\square$ ) would be adequate for antistatic purposes where values below  $5 \cdot 10^9 \Omega/\square$  are needed. As in EIS, CV also showed an increase in the electro-activity with the number of RGO layers. With only one RGO coating, the contact between the different RGO sheets is not

satisfactory and more layers are needed to improve this contact and obtain a material with good electrical and electrochemical properties. Scan rate is also a key parameter in the characterization of these materials and only low scan rates allow the best observation of redox processes. Approach curves and maps of electro-activity obtained by SECM showed the clear difference between levels of electro-activity of PES-GO and PES-RGO samples. The electrochemical techniques used for the characterization indicate the need to apply several RGO coatings during the synthesis to obtain materials with the best electrical and electrochemical properties.

### **Acknowledgements**

The authors wish to thank the Spanish Ministerio de Ciencia e Innovación (contracts CTM2010-18842-C02-02 and CTM2011-23583) and Universitat Politècnica de València (Vicerrectorado de Investigación PAID-06-10 contract 003-233) for their financial support. J. Molina is grateful to the Conselleria d'Educació (Generalitat Valenciana) for the FPI fellowship. A.I. del Río is grateful to the Spanish Ministerio de Ciencia y Tecnología for the FPI fellowship.

### **References**

- [1] KS Novoselov, AK Geim, SV Morozov, D Jiang, Y Zhang, SV Dubonos, IV Grigorieva, AA Firsov, Electric field effect in atomically thin carbon film, *Science* 306 (2004) 666.
- [2] AK Geim, KS Novoselov, The rise of graphene, *Nat Mater* 6 (2007)183.
- [3] AK Geim, Graphene: status and prospects, *Science* 324 (2009) 1530.

- [4] AH Castro Neto, F Guinea, NMR Peres, KS Novoselov, AK Geim, The electronic properties of graphene, *Rev Mod Phys* 81 (2009) 109.
- [5] HB Heersche, P Jarillo-Herrero, JB Oostinga, LMK Vandersypen, AF Morpurgo, Bipolar supercurrent in graphene, *Nature* 446 (2007) 56.
- [6] MJ Allen, VC Tung, RB Kaner, Honeycomb carbon: A review of graphene, *Chem Rev* 110 (2010)132.
- [7] C Soldano, A Mahmood, E Dujardin, Production, properties and potential of graphene, *Carbon* 48 (2010) 2127.
- [8] V Singh, D Joung, L Zhai, S Das, SI Khondaker, S Seal, Graphene based materials: Past, present and future, *Prog Mater Sci* 56 (2011) 1178.
- [9] S Park, RS Ruoff, Chemical methods for the production of graphenes, *Nat Nanotechnol* 4 (2009) 217.
- [10] JR Potts, DR Dreyer, CW Bielawski, RS Ruoff, Graphene-based polymer nanocomposites, *Polymer* 52 (2011) 5.
- [11] J Molina, MF Esteves, J Fernández, J Bonastre, F Cases, Polyaniline coated conducting fabrics. Chemical and electrochemical characterization, *Eur Polym J* 47 (2011) 2003.
- [12] J Molina, AI del Río, J Bonastre, F Cases, Chemical and electrochemical polymerisation of pyrrole on polyester textiles in presence of phosphotungstic acid, *Eur Polym J* 44 (2008) 2087.
- [13] S Gowri, L Almeida, T Amorim, N Carneiro, AP Souto, MF Esteves. Polymer nanocomposites for multifunctional finishing of textiles - a review. *Text Res J* 80 (2010) 1290.
- [14] L Hu, M Pasta, F La Mantia, L Cui, S Jeong, HD Deshazer, JW Choi, SM Han, Y Cui, Stretchable, porous, and conductive energy textiles, *Nano Lett* 10 (2010) 708.

- [15] G Yu, L Hu, M Vosgueritchian, H Wang, X Xie, JR McDonough, X Cui, Y Cui, Z Bao, Solution-processed graphene/MnO<sub>2</sub> nanostructured textiles for high-performance electrochemical capacitors, *Nano Lett* 11 (2011) 2905.
- [16] B Fugetsu, E Sano, H Yu, K Mori, T Tanaka, Graphene oxide as dyestuffs for the creation of electrically conductive fabrics, *Carbon* 48 (2010) 3340.
- [17] W Gu, Y Zhao, Graphene modified cotton textiles, *Adv Mat Res* 331 (2011) 93.
- [18] K Krishnamoorthy, U Navaneethaiyer, R Mohan, J Lee, SJ Kim, Graphene oxide nanostructures modified multifunctional cotton fabrics, *Appl Nanosci* 2 (2012) 119.
- [19] X Li, P Sun, L Fan, M Zhu, K Wang, M Zhong, J Wei, D Wu, Y Cheng, H Zhu, Multifunctional graphene woven fabrics, *Sci Rep* 2 (2012) 395.
- [20] Z Xu, C Gao, Graphene chiral liquid crystals and macroscopic assembled fibres, *Nat Commun* 2 (2011) 571.
- [21] Z Dong, C Jiang, H Cheng, Y Zhao, G Shi, L Jiang, L Qu, Facile fabrication of light, flexible and multifunctional graphene fibers, *Adv Mater* 24 (2012) 1856.
- [22] P Sun, FO Laforge, MV Mirkin, Scanning electrochemical microscopy in the 21st century, *Phys Chem Chem Phys* 9 (2007) 802.
- [23] MV Mirkin, BR Horrocks, Electroanalytical measurements using the scanning electrochemical microscope, *Anal Chim Acta* 406 (2000) 119.
- [24] AL Barker, M Gonsalves, JV Macpherson, CJ Slevin, PR Unwin, Scanning electrochemical microscopy: beyond the solid/liquid interface, *Anal Chim Acta* 385 (1999) 223.
- [25] RM Souto, JJ Santana, L Fernández-Mérida, S González, Sensing electrochemical activity in polymer coated metals during the early stages of coating degradation—Effect of the polarization of the substrate, *Electrochim Acta* 56 (2011) 9596.

- [26] Complete textile glossary, available from: [http://www.celaneseacetate.com/textile\\_glossary\\_filament\\_acetate.pdf](http://www.celaneseacetate.com/textile_glossary_filament_acetate.pdf), 2001. Last accessed 15th October 2012.
- [27] J Molina, J Fernández, AI del Río, R Lapuente, J Bonastre, F Cases, Stability of conducting polyester/polypyrrole fabrics in different pH solutions. Chemical and electrochemical characterization, *Polym Degrad Stab* 95 (2010) 2574.
- [28] J Molina, J Fernández, AI del Río, J Bonastre, F Cases, Chemical, electrical and electrochemical characterization of hybrid organic/inorganic polypyrrole/ $\text{PW}_{12}\text{O}_{40}^{3-}$  coating deposited on polyester fabrics, *Appl Surf Sci* 257 (2011) 10056.
- [29] EY Choi, TH Han, J Hong, JE Kim, SH Lee, HW Kim, SO Kim, Noncovalent functionalization of graphene with end-functional polymers, *J Mater Chem* 20 (2010) 1907.
- [30] DC Marcano, DV Kosynkin, JM Berlin, A Sinitskii, Z Sun, A Slesarev, LB Alemany, W Lu, JM Tour, Improved synthesis of graphene oxide, *ACS Nano* 4 (2010) 4806.
- [31] Y Si, ET Samulski, Synthesis of water soluble graphene, *Nano Lett* 8 (2008) 1679.
- [32] S Park, RS Ruoff, Chemical methods for the production of graphenes, *Nat Nanotechnol* 4 (2009) 217.
- [33] P Lian, X Zhu, S Liang, Z Li, W Yang, H Wang, Large reversible capacity of high quality graphene sheets as an anode material for lithium-ion batteries, *Electrochim Acta* 55 (2010) 3909.
- [34] DR Dreyer, S Park, CW Bielawski, RS Ruoff, The chemistry of graphene oxide, *Chem Soc Rev* 39 (2010) 228.
- [35] T Textor, B Mahltig, A sol-gel based surface treatment for preparation of water repellent antistatic textiles, *Appl Surf Sci* 256 (2010) 1668.

- [36] AT Valota, IK Kinloch, KS Novoselov, C Casiraghi, A Eckmann, EW Hill, RAW Dryfe, Electrochemical behavior of monolayer and bilayer graphene, ACS Nano 5 (2011) 8809.
- [37] W Li, C Tan, MA Lowe, HD Abruña, DC Ralph, Electrochemistry of individual monolayer graphene sheets, ACS Nano 5 (2011) 2264.
- [38] L Rajendran, SP Ananthi, Analysis of positive feedback currents at the scanning electrochemical microscope, J Electroanal Chem 561 (2004) 113.
- [39] AJ Bard, MV Mirkin, Scanning Electrochemical Microscopy, Marcel Dekker Inc, New York, 2001.
- [40] C Tan, J Rodríguez-López, JJ Parks, NL Ritzert, DC Ralph, HD Abruña, Reactivity of monolayer chemical vapor deposited graphene imperfections studied using scanning electrochemical microscopy, ACS Nano 6 (2012) 3070.
- [41] AG Güell, N Ebejer, ME Snowden, JV Macpherson, PR Unwin, Structural correlations in heterogeneous electron transfer at monolayer and multilayer graphene electrodes, J Am Chem Soc 134 (2012) 7258.
- [42] J Rodríguez-López, NL Ritzert, JA Mann, C Tan, WR Dichtel, HD Abruña, Quantification of the surface diffusion of tripodal binding motifs on graphene using scanning electrochemical microscopy, J Am Chem Soc 134 (2012) 6224.

### Figure captions

Fig. 1. FTIR-ATR spectra of GO and RGO powders. Resolution  $4\text{ cm}^{-1}$ , 100 scans.

Fig. 2. Micrographs of: (a) PES-1G x10000; (b) PES-1G x10000; (c) PES-4G x100; (d) PES-4G x2000.

Fig. 3. Bode plots for PES, PES-GO, PES-1G, PES-2G, PES-3G and PES-4G. Sample located between two copper electrodes. Frequency range from  $10^5$  Hz to  $10^{-2}$  Hz.

Fig. 4. Magnified dependence of the impedance modulus on ac frequency for: a) PES-1G, b) PES-2G, c) PES-3G and d) PES-4G. Sample located between two copper electrodes. Frequency range from  $10^5$  Hz to  $10^{-2}$  Hz.

Fig. 5. Cyclic voltammograms of: a) PES-1G without ohmic compensation, b) PES-3G without ohmic compensation, c) PES-3G with ohmic resistance compensation, third scan for all measurements. 0.5 M  $\text{H}_2\text{SO}_4$  (pH~0) Scan rates used: 50, 5 and 1  $\text{mV s}^{-1}$ .

Fig. 6. Cyclic voltammogram obtained with a 100  $\mu\text{m}$  Pt SECM-tip in a 0.01 M  $\text{Ru}(\text{NH}_3)_6^{3+}$  and 0.1 M KCl solution, scan rate 50  $\text{mV s}^{-1}$ .

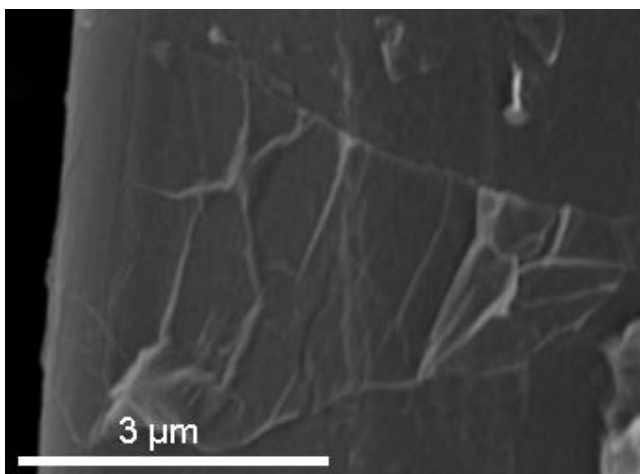
Fig. 7. Approaching curves for: PES (····), PES-GO (continuous lines) and theoretical negative feedback model ( $\square$ ). Obtained with a 100  $\mu\text{m}$  diameter SECM-tip in 0.01 M  $\text{Ru}(\text{NH}_3)_6^{3+}$  and 0.1 M KCl. The tip potential was -400 mV (vs Ag/AgCl) and the approach rate was 10  $\mu\text{m s}^{-1}$ .

Fig. 8. Approaching curves for: a) PES-1G (continuous lines), theoretical positive feedback model ( $\Delta$ ) and b) PES-4G (continuous lines), theoretical positive feedback model ( $\Delta$ ). Obtained with a 100  $\mu\text{m}$  diameter Pt SECM-tip in 0.01 M  $\text{Ru}(\text{NH}_3)_6^{3+}$  and

0.1 M KCl. The tip potential was -400 mV (vs Ag/AgCl) and the approach rate was 10  $\mu\text{m s}^{-1}$ .

Fig. 9. 3D (a,c) and 2D (b,d) constant height SECM images of: PES-1G sample (a,b), PES-GO sample. 0.25  $\text{cm}^2$  geometrical area sample, images were taken with a 100  $\mu\text{m}$  diameter Pt SECM-tip, in 0.01 M  $\text{Ru}(\text{NH}_3)_6^{3+}$  at a constant height. The tip potential was -400 mV, the scan rate was 200  $\mu\text{m s}^{-1}$  in comb mode; lengths of x and y lines were 1500 x 1500  $\mu\text{m}$  with increments of 50  $\mu\text{m}$ .

Fig. 10. Superposition of the 2D SECM array and a SEM micrograph for a PES-1G sample.

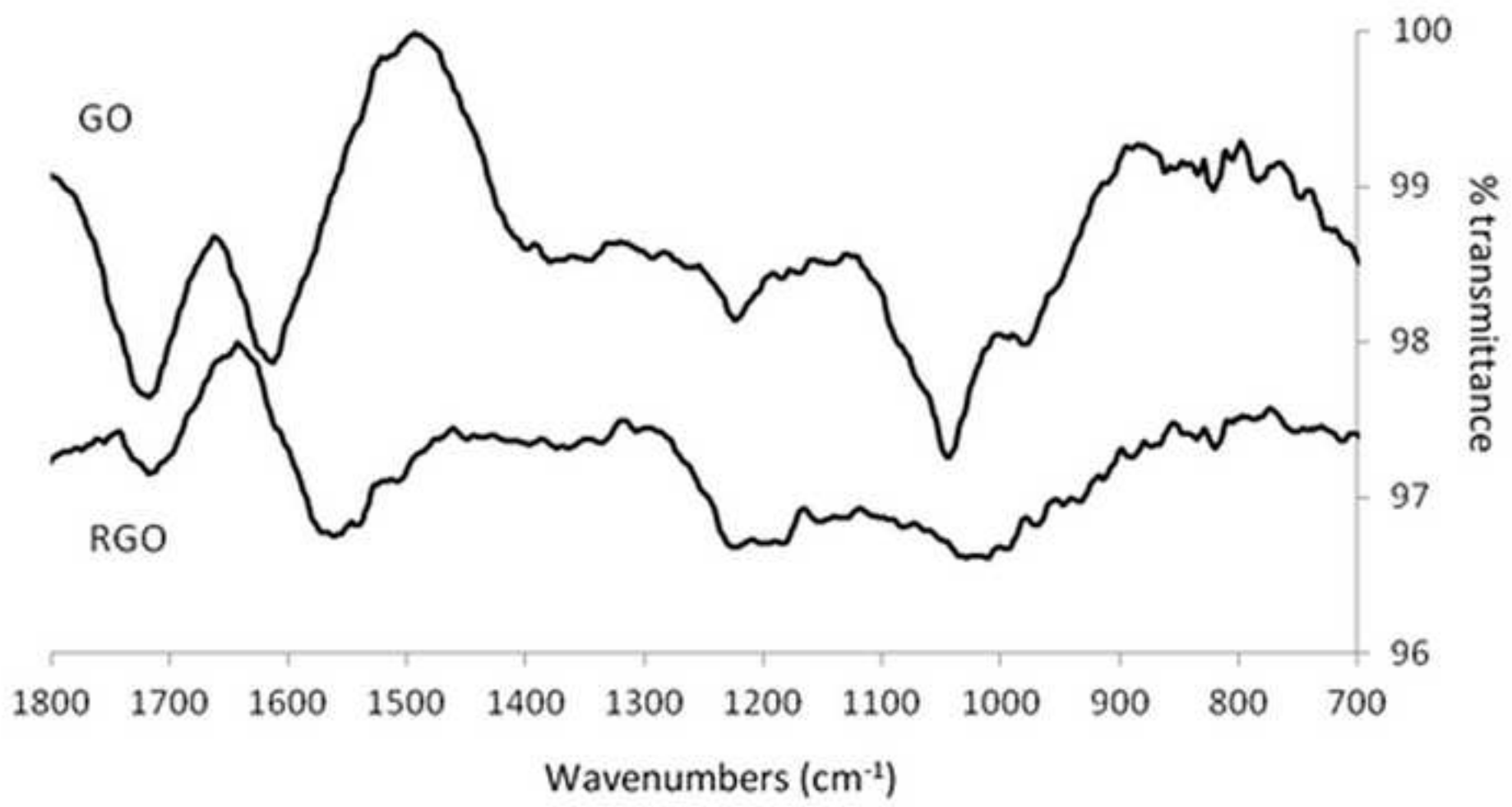


Accepted Manuscript

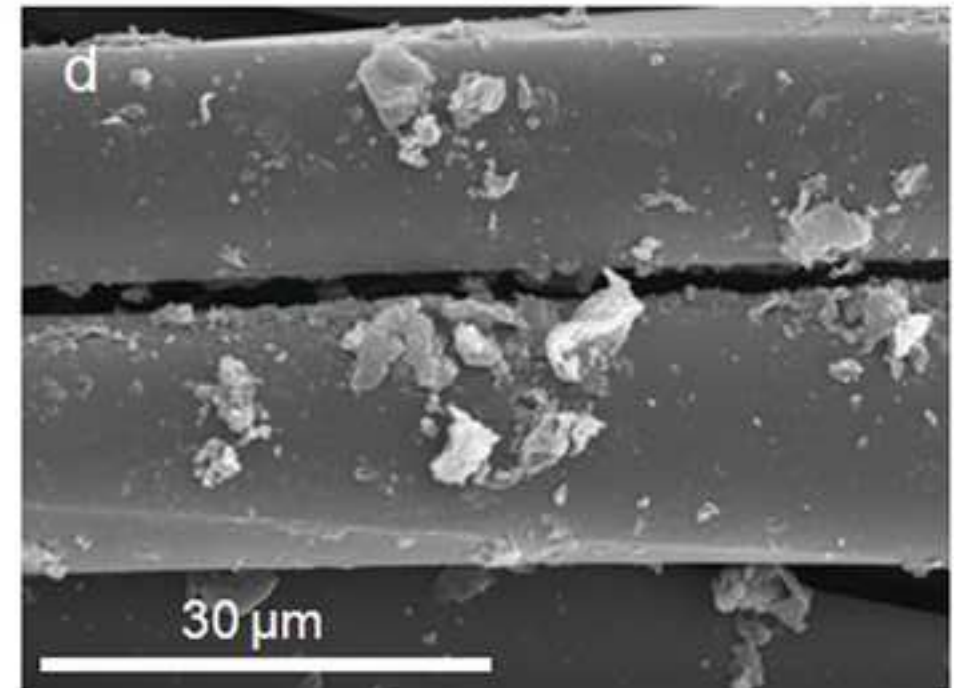
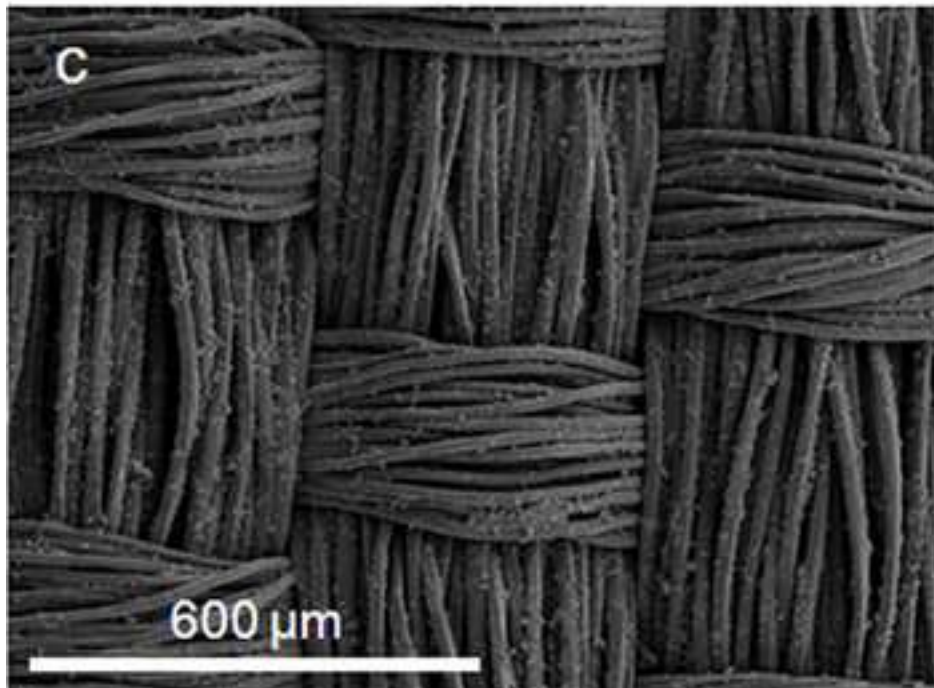
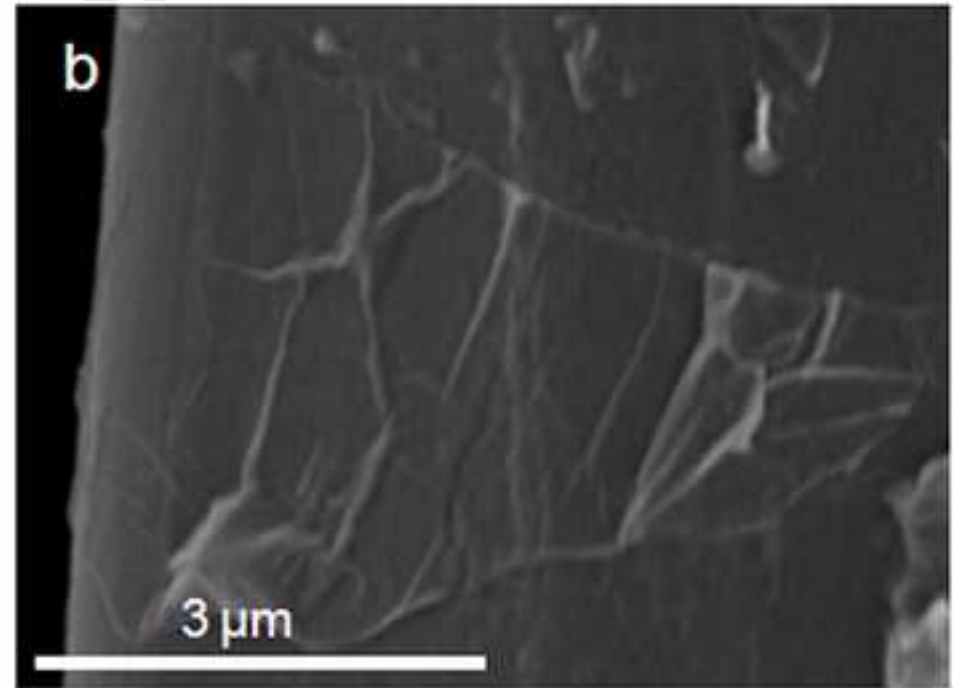
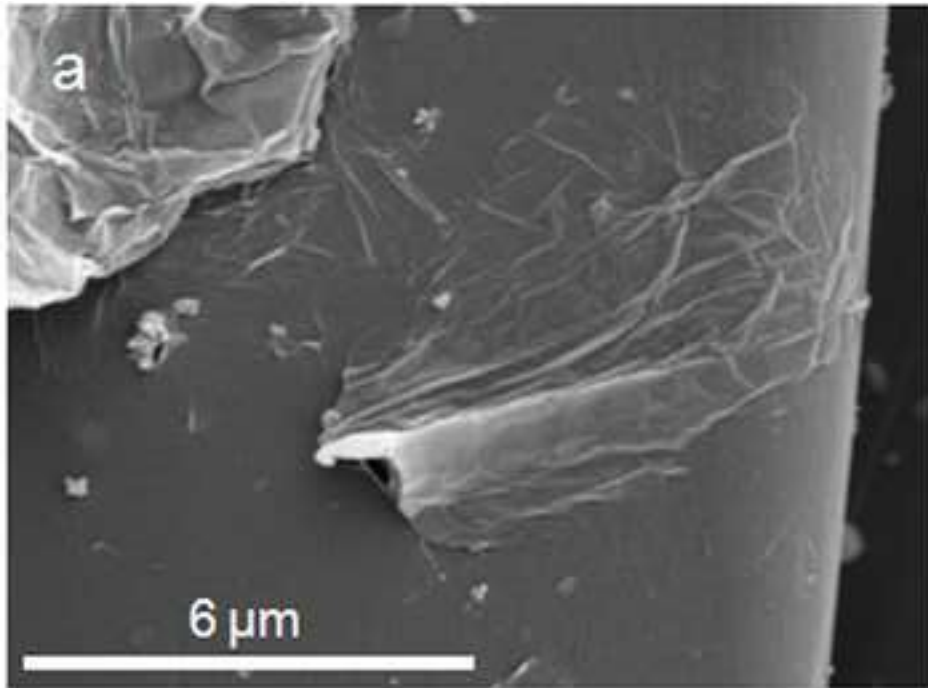
**Highlights:**

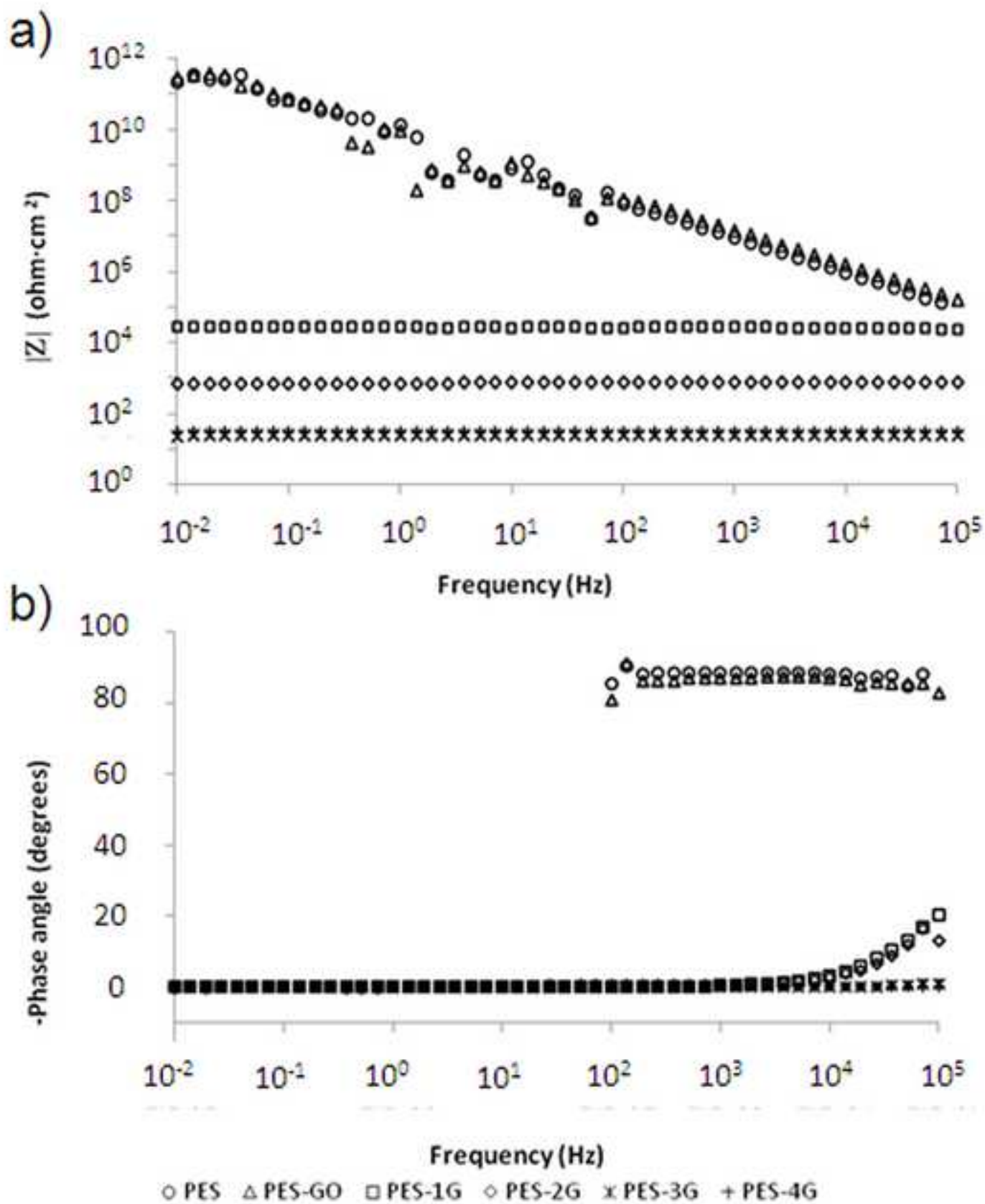
- Graphene-coated fabrics have been obtained by chemical reduction of graphene oxide.
- Conducting fabrics have been obtained applying several graphene coatings.
- Electrochemical impedance spectroscopy showed the conductive behaviour of fabrics.
- Scan rate is a key parameter in the characterization by cyclic voltammetry.
- Scanning electrochemical microscopy showed the increase of electroactivity.

Figure(1)

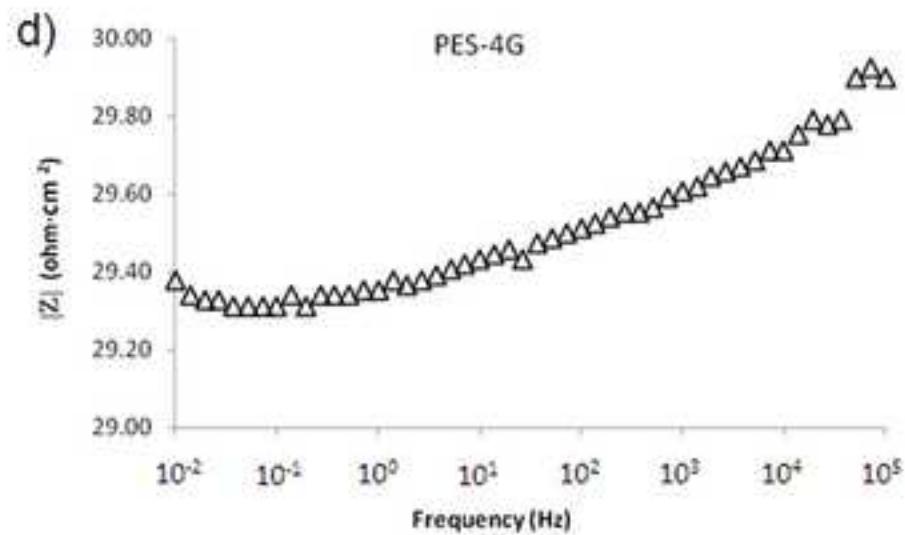
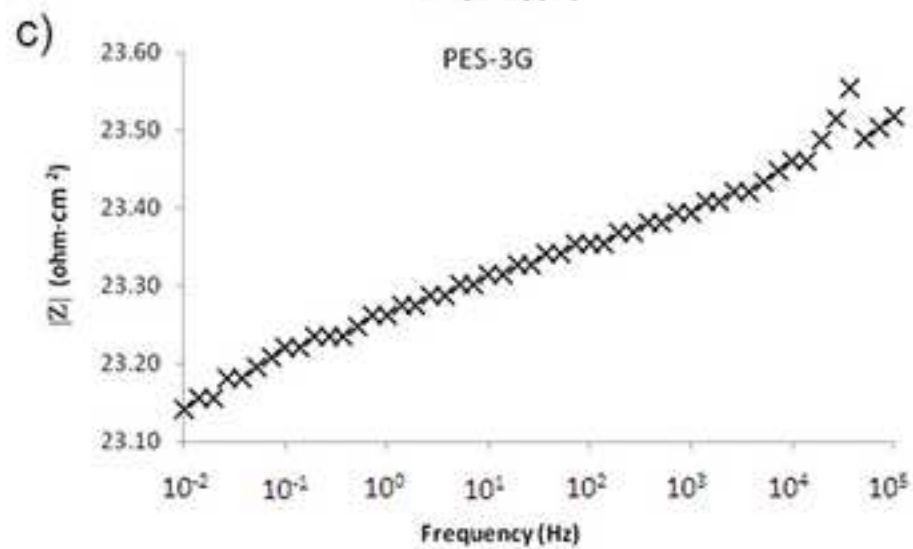
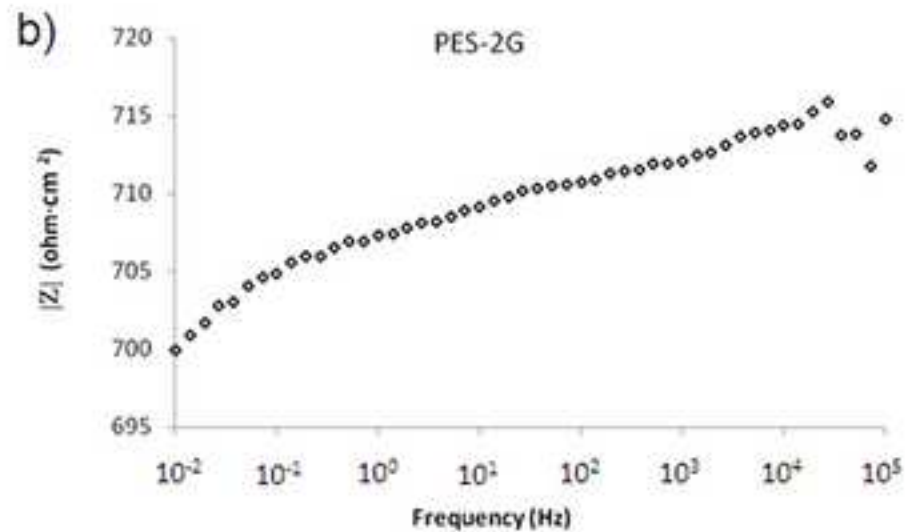
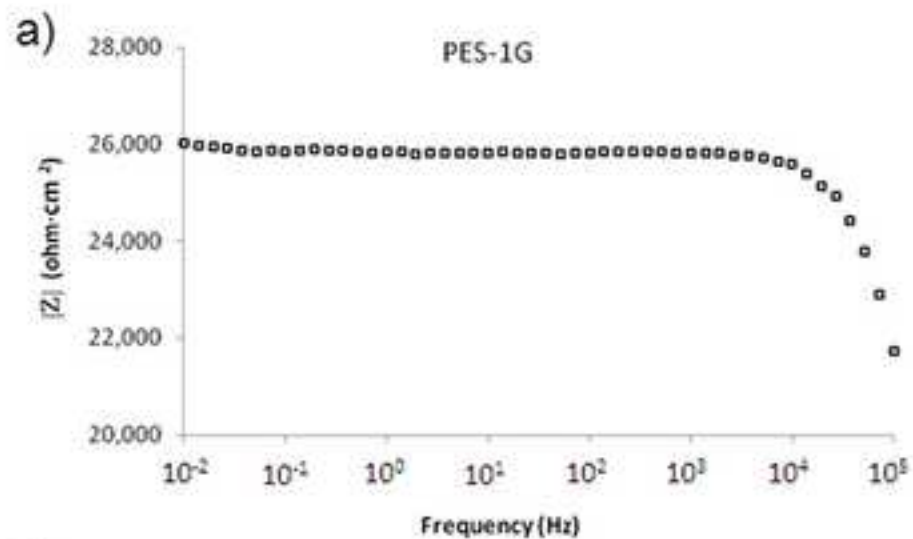


Figure(2)



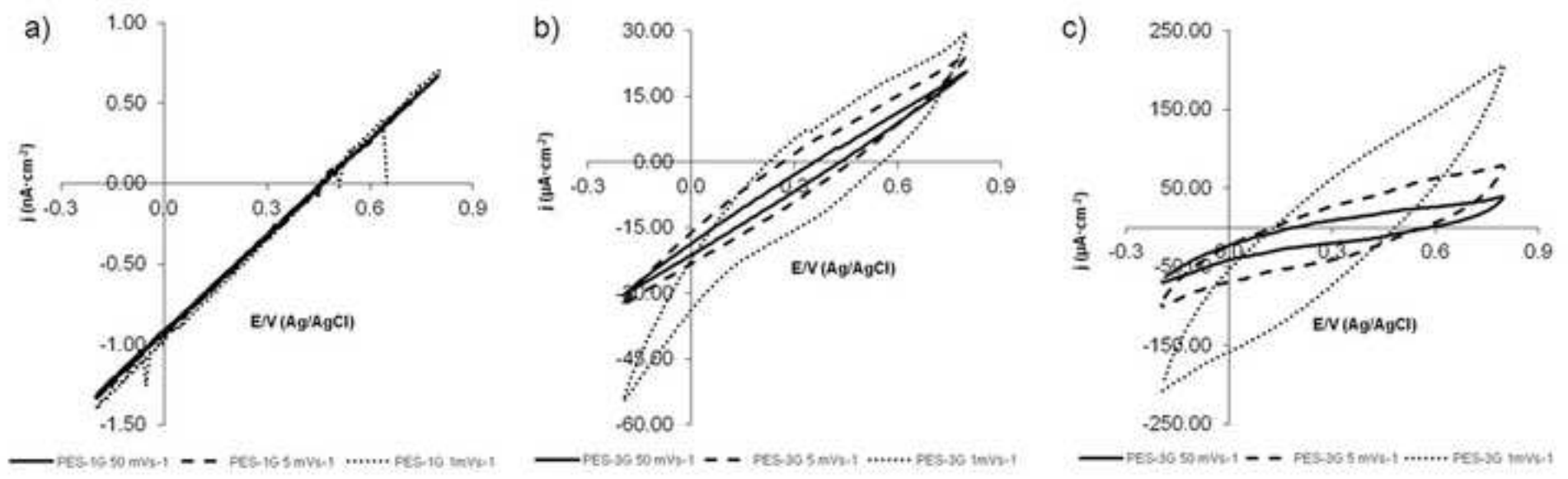


Figure(4)

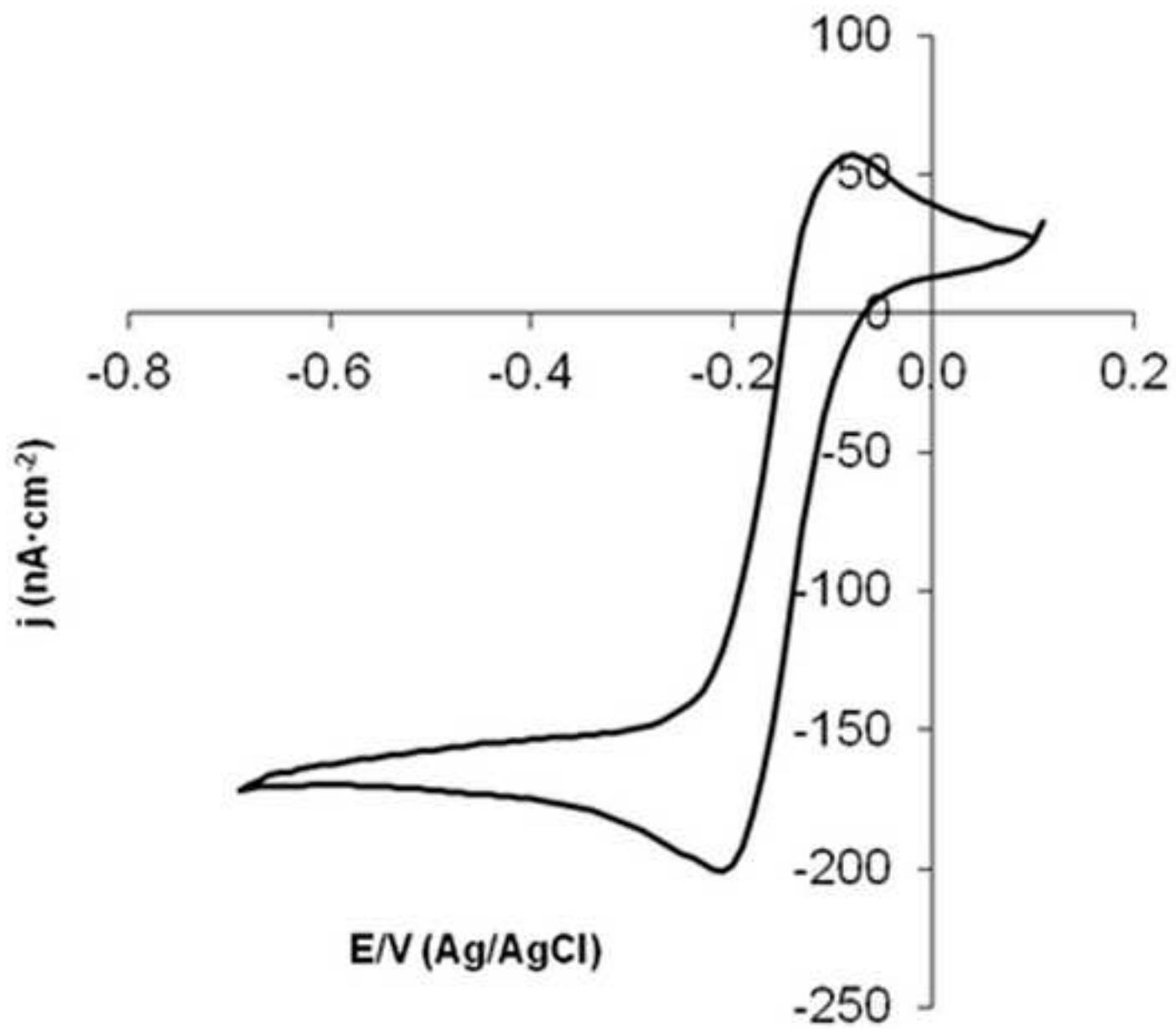


Figure(5)

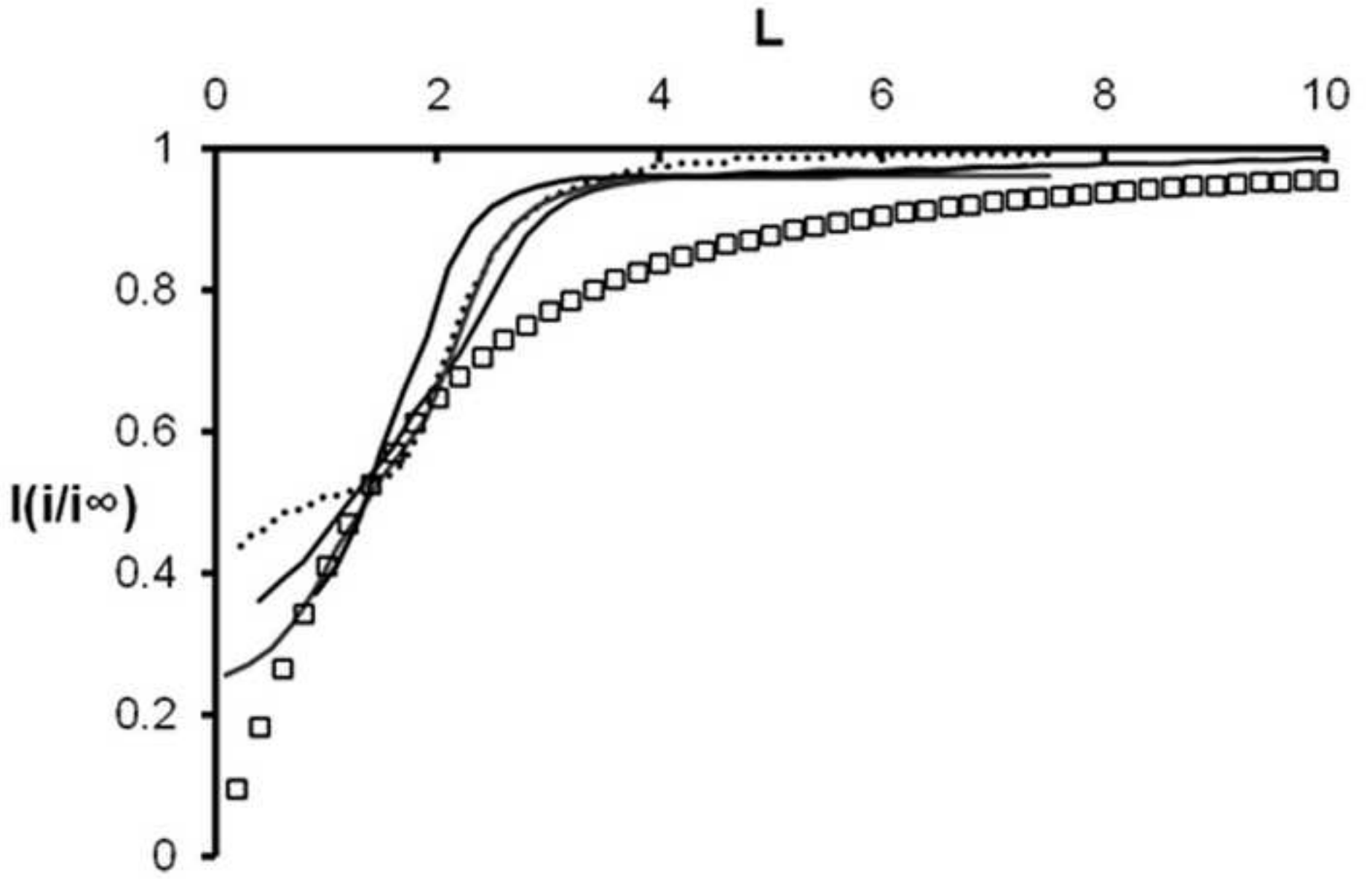
Manuscript

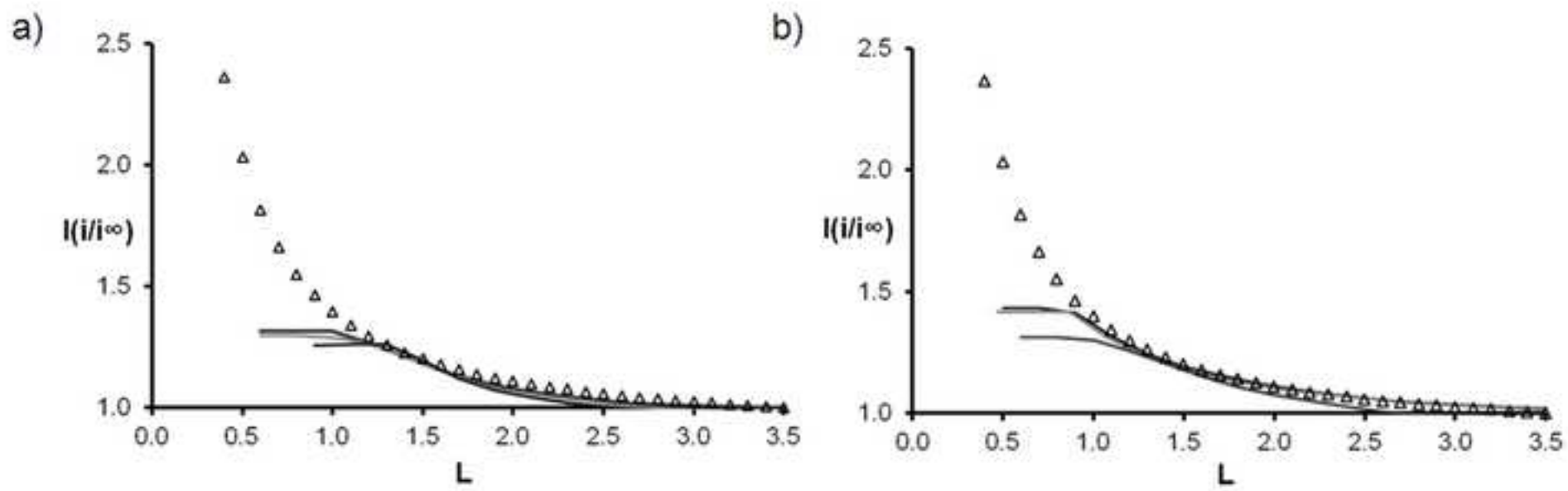


Figure(6)



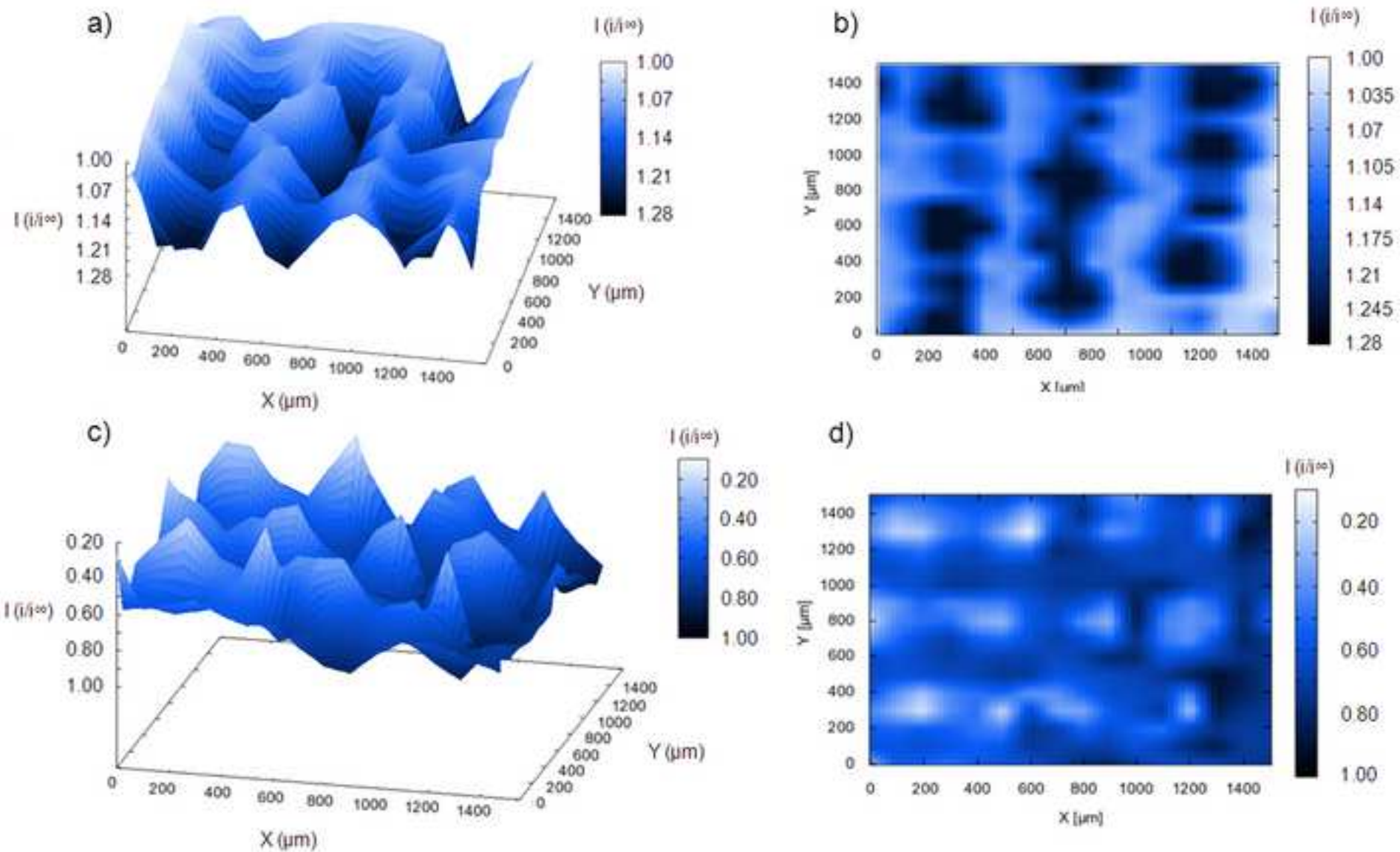
Figure(7)





Figure(9)

scrip



Figure(10)

scrip

